A Compact, Batteryless, and Chipless Intermodulation Sensor for Wireless Crack Detection

Xuecong Nie, Nanshu Wu, Chung-Tse Michael Wu, *Senior Member, IEEE*, and Pai-Yen Chen, *Senior Member, IEEE*

***Abstract*—In this article, we introduce a wireless nondestructive evaluation (NDE) technique that exploits intermodulation interrogation from a compact, fully passive nonlinear antenna sensor, so as to suppress electromagnetic interreferences, such as clutters, echoes, and self-jamming. The antenna sensor consists of a local oscillator and a passive rectifier/mixer, connected to a microstrip patch antenna whose resonance frequency is sensitively tuned by the surface crack level (i.e., cavity perturbation). This nonlinear antenna sensor receives a frequency-hopped radio frequency (RF) monotone from the interrogator and reradiates an intermodulation signal produced by mixing the input RF signal (2.4 GHz) and the low-frequency signal (1.0–1.2 MHz) generated by the local oscillator. Through the frequency-hopped spread spectrum (FHSS) interrogation, the spectral signal strength pattern can identify the crack level encoded in the resonance frequency shift of the microstrip antenna. Compared with other nonlinear wireless sensors, such as harmonic/subharmonic sensors, the proposed intermodulation-based antenna sensor not only enables clutter-resistive passive wireless sensing, but also provides several advantages. First, it can significantly reduce the size and cost of the sensor and interrogator by removing high-harmonic antennas and reducing the design complexity of the interrogator. Second, it provides digital memory-free identification by assigning the oscillation frequency as the sensor's identification (ID) key. Additionally, receiving intermodulation signals rather than harmonic tones can reduce the path loss and thus increase the wireless interrogation distance. The proposed fully passive intermodulation-based antenna sensor may open a new path to build portable, low-cost, low-noise, energy-efficient wireless pervasive NDE platforms.**

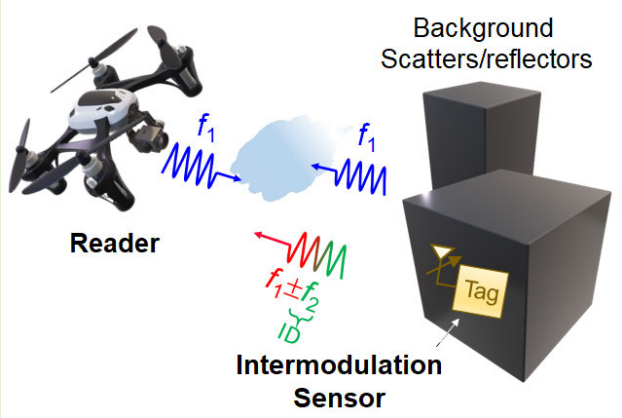

***Index Terms*— Antenna sensor, intermodulation, microstrip antennas, radio frequency identification (RFID), structural health monitoring (SHM), wireless crack sensor.**

I. Introduction

STRUCTURAL health monitoring (SHM) for fatigue cracks and advent in the Internet of Things (IoT), smart SHM system strain is of great importance in the risk assessment of civil and industrial infrastructures, as surface cracks could potentially give rise to economic losses and threaten human safety [1], [2]. Traditional time-based maintenance generally relies on thorough on-site inspections and laboratory experiments, which require high labor and material costs [3]. Moreover, some internal inspections could cause unpredictable damage to the structure. In recent years, there has been growing research interest for the development of a cost-effective nondestructive evaluation (NDE) system, capable of continuous, real-time monitoring of fatigue cracks [4], [5]. With the rapid advent of IoT, smart SHM systems connected to wireless sensor networks have been proposed to monitor infrastructure conditions wirelessly and consciously, thereby significantly reducing the mandatory maintenance period and labor cost [2], [6], [7], [8]. These emerging radio frequency (RF) SHM sensors include RF identification (RFID) crack sensors [9], antenna-based crack sensors [10], battery-assisted active IoT nodes [12], [13], [14], eddy current testing (ECT) [15], [16], [17], and harmonic crack sensors [18], [19], to name a few. However, most of them suffer from one or more significant flaws, such as low sensitivity, short

Manuscript received 28 January 2024; revised 19 February 2024; accepted 19 February 2024. Date of publication 27 February 2024; date of current version 2 April 2024. This work was supported by NSF under Grant ECCS 2229659. The associate editor coordinating the review of this article and approving it for publication was Dr. Wensong Wang. *(Corresponding author: Pai-Yen Chen.)*

Xuecong Nie, Nanshu Wu, and Pai-Yen Chen are with the Department of Electrical and Computer Engineering, University of Illinois Chicago, Chicago, IL 60607 USA (e-mail: pychen@uic.edu).

Chung-Tse Michael Wu is with the Department of Electrical and Computer Engineering, Rutgers University, New Brunswick, NJ 08854 USA (e-mail: ctm.wu@rutgers.edu).

Digital Object Identifier 10.1109/JSEN.2024.3368332

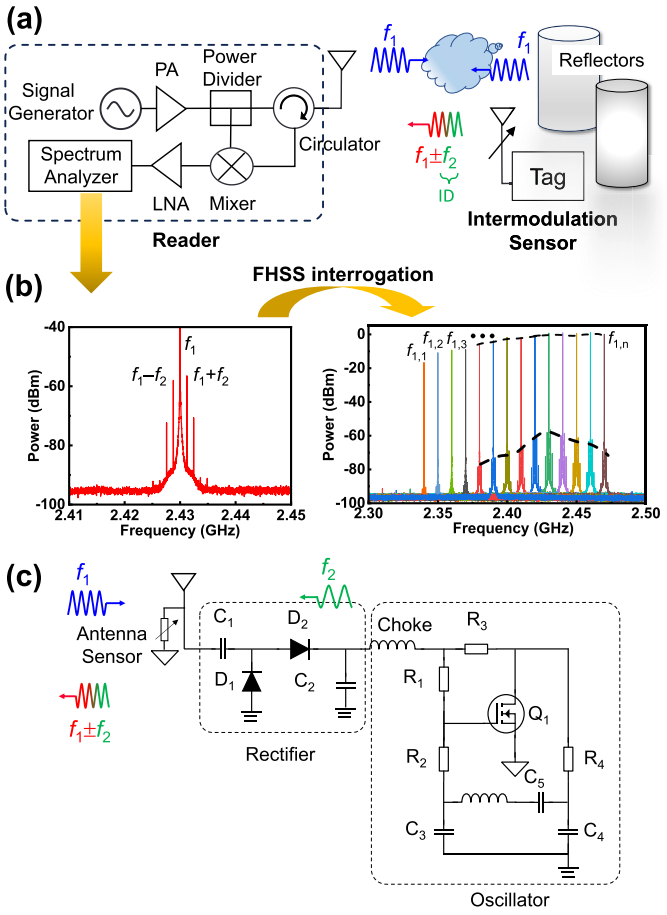

Fig. 1. (a) Schematic of the passive and nonlinear wireless crack sensor based on the intermodulation readout and (b) its spectral response (RSSI) at the fundamental and intermodulation frequencies. (c) Schematic of the intermodulation sensor circuit elements.

detection range (e.g., ECT), and high maintenance cost due to the limited battery lifetime and sustainability (e.g., active IoT crack sensors). Also, passive wireless sensors generally have a poor signal-to-noise ratio (SNR) due to clutters, multipath interreferences, and self-jamming when considering real-world infrastructures with various large scatters. Although passive harmonic transponder sensors can overwhelm the unwanted clutters and jamming in noisy environments and require no power supply, their practical implementation is rather sophisticated, especially regarding the interrogator design that deals with both RF fundamental and harmonic bands.

To address the abovementioned issues, we introduce herein a clutter-immune, fully passive, and chipless wireless crack sensor and the frequency-hopped spread spectrum (FHSS)-aided intermodulation readout system, as illustrated in Fig. 1(a). The wireless crack sensor consists of a voltage rectifier/mixer, a local oscillator, and a microstrip patch antenna. When the sensor, which is conformably attached to the targeted metallic surfaces, receives the RF interrogation signal at frequency f_1 (2.3–2.5 GHz), the passive diode-based rectifier coverts the RF input signal into a dc voltage to power up the local oscillator, generating a low-frequency signal at frequency f_2 (1.08 MHz). The nonlinear diode rectifier also acts as a passive mixer to generate intermodulation products $f_1 \pm n{\cdot}f_2$, where n is an integer. Finally, the narrowband microstrip patch antenna, which serves as a sensor and a high-Q bandpass filter, retransmits the intermodulation signal to the interrogator or sniffer. The concept of the FHSS-based wireless crack sensing is illustrated in Fig. 1(b). An interrogator transmits a frequency-hopped RF signal to the infrastructure equipped with the passive intermodulation sensor. The interrogating signal has a hopping sequence covering channels $[f_{11}, f_{12}, \ldots, f_{1n}]$ with constant signal strength [20], [21]. If there exists a crack on the metal object (i.e., the ground plane of the patch antenna), the FHSS pattern over channels $[f_{11}-f_2, f_{12}-f_2, \ldots, f_{1n}-f_2]$ of the intermodulation received signal strength indicator (RSSI) at the interrogator or sniffer will signify the resonance profile of the antenna sensor (which is a strong function of the crack level). The intermodulation process is necessary because at the carrier frequencies, there is strong direct coupling from the interrogator and to the receiver/sniffer, as well as background scattering (e.g., clutters, multipath scattering, and other electromagnetic interferences) in noisy environments. In addition, intermodulation signals are exclusively in the spectrum and, thus, are much cleaner, yielding a low SNR. Compared to sensors with 1-D data, which relies on the signal amplitude, the high-dimensional RSSI vector provides abundant information to enable pattern analysis-based decoding, thereby enabling robust and absolute accuracy crack sensing. Maintenance or replacement should be prioritized if the peak frequency of the intermodulation RSSI pattern has a drastic shift due to cracks. Since the proposed sensor and system are potentially lightweight and low cost, a portable interrogator can be used to detect and decode the sensing signals and can be connected to the cloud-based data center that serves as the hub for storing the SHM information and maintenance scheduling. Compared with the harmonic RFID systems [22], [23], [24], [25] that are commonly used to counter clutters in rich-scattering environments, the proposed intermodulation sensor not only reduces the design complexity of the interrogator, but also reduces the sensor size by removing the antenna, filter, and matching network operating at the harmonic frequency. Moreover, the local oscillator frequency in the low-frequency (tens of kHz to several MHz) band can be exploited to identify different sensor nodes in a network, i.e., the oscillation frequency represents the sensor's identification (ID) key. We should emphasize that each sensor can be readily assigned to a specific oscillation frequency by tuning the LC resonator of the local oscillator. Finally, since frequencies of intermodulation products are close to that of the RF interrogation signal, the interrogation distance can be enhanced when compared with harmonic sensors that typically suffer from a higher propagation loss at the harmonic frequency. In the following, we will detail the design and implementation of the proposed wireless crack sensor and integrated system.

II. Design and Practical Implementation of Intermodulation Sensor

A. FHSS-Aided Intermodulation Sensor and System

Fig. 1 depicts the schematic of the proposed passive intermodulation sensor and the FHSS pattern analysis-based crack

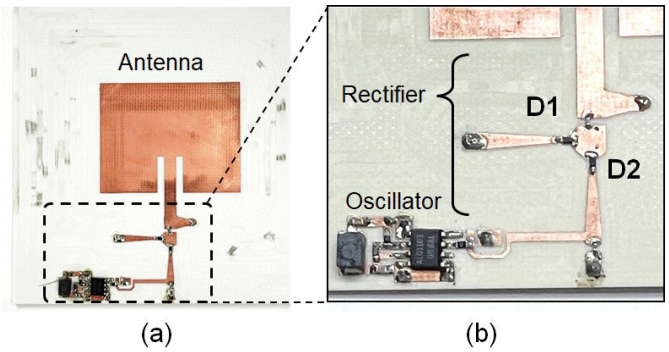

Fig. 2. (a) Photograph of the nonlinear antenna sensor that receives an RF monotone (2.4 GHz) and retransmits an intermodulation tone (2.4 GHz ± few MHz). (b) Zoomed-in view of the rectifier and local oscillator on the antenna sensor in (a).

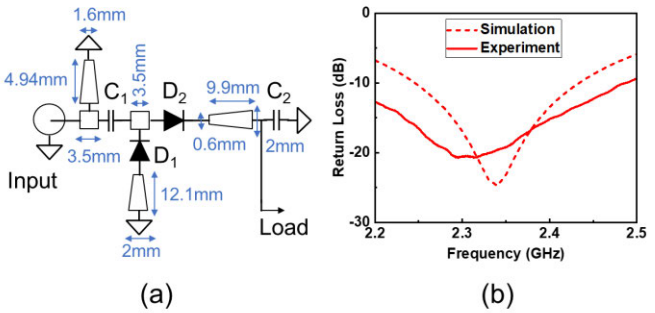

Fig. 3. (a) Distributed matching elements physical dimensions and circuit diagram and (b) return loss (dB) of the rectifier/mixer in Fig. 1 at an input RF power level of −15 dBm.

sensing system. The interrogator prototype has a tunable RF signal generator, a spectrum analyzer, a circulator, and an ultrawide-band (UWB) antenna. The interrogator transmits a frequency-hopped RF monotone to power up the wireless passive crack sensor, which consists of a low-profile microstrip patch antenna (which also acts as the sensing element), a rectifier/mixer, and an oscillator, as shown in Fig. 2. The dc output voltage of the diode rectifier is used to bias and activate the local oscillator to generate a local signal at 1.08 MHz. Finally, the local oscillation signal is mixed with the input RF signal to generate the intermodulation signal $f_1 \pm f_2$, which is retransmitted to the interrogator by the same patch antenna. A circulator on the interrogator can then separate backscattered signals at f_1 and $f_1 \pm f_2$, and the latter one will be downconverted to f_2 by a mixer. In addition, harmonic signals that may be generated on the nonlinear antenna sensor can be rejected by the narrowband nature of the microstrip patch antenna, as well as the antialiasing filter in the spectrum analyzer. Fig. 1 presents the circuit schematic of the passive intermodulation sensor, of which the patch antenna also functions as a crack sensor. A microstrip patch antenna can be viewed as an open cavity with four perfect magnetic conductor (PMC) walls, and, therefore, it typically has a high Q-factor and strongly localized electric fields. According to the cavity perturbation theory [26], [27], the surface crack or deformation appearing on the metallic ground plane of the antenna will vary the resonance frequency of such an open cavity. As a result, the resonance frequency of the patch antenna may be sensitively dependent on the crack size. Here, the rectifier is based on a passive two-diode voltage doubler architecture [28], and the local oscillator is modified from the Colpitts oscillator [29]. Initially, for a pristine sample without fatigue cracks, the peak of the intermodulation RSSI pattern at $f_1 - f_2$ is locked at 2.43 GHz. Once the fatigue crack occurs, the resonance frequency of the microstrip patch antenna shifts, which can be detected by tracking the corresponding peak frequency in the intermodulation RSSI pattern [see Fig. 1(b)]. Subsequently, the crack level can be detected through observation of the change in the peak frequency of the intermodulation RSSI. The design of key components in the intermodulation sensor is detailed in the following.

B. RF Circuits for Passive Intermodulation

Figs. 2(b) and 3(a) show the photograph and the circuit diagram of the proposed RF rectifier/mixer, which was built using zero-bias Schottky diodes (Skyworks SMS7630-05F), transmission-line segments, and chip capacitors with their capacitance values given by $C_1 = 18$ pF and $C_2 = 22$ pF. The input of the rectifier/mixer is matched to 50 Ω over the interested band (2.2–2.5 GHz), which fully covers the antenna's operating frequency. Fig. 3(b) shows the reflection coefficient of the proposed rectifier, which is lower than −10 dB across the frequency band of interest. The rectifier circuit was manufactured on the 1.52-mm-thick Rogers 4003C printed-circuit board with 1-oz electrodeposited copper foil by using the LPKF E44 circuit board plotter. Fig. 4(a) shows the schematic of the local oscillator that generates a sinusoidal output wavefront at 1.08 MHz at −13.7-dBm RF input power. The oscillator was built based on the Colpitts-type topology with important design parameters provided by commercial lumped elements: $C_3 = 7.2$ pF, $C_4 = 36$ pF, $L_1 = 1$ mH, $R_1 = 1.2$ MΩ, $R_2 = 2$ Ω, and $R_3 = 10$ kΩ, where the frequency of oscillation is determined by C_3, C_4, and L_1 on the resonant tank. Here, the RF choke is a miniature surface mount ferrite bead, and the coupling capacitor C_5 is a 100-nF ceramic capacitor. The local oscillator is powered by a rectifier shown in Fig. 3. Here, we should note that this oscillator is designed to operate at low supply voltage and low power consumption, ensuring a long interrogation distance for the far-field passive readout. The minimum operating voltage of most commercial LVCMOS oscillators is generally higher than 1.8 V, which may not be suitable for long-range interrogation. To increase the system's maximum interrogation range, we designed and fabricated a low-frequency local oscillator using ALD110900 MOSFET from Advance Linear Device, Sunnyvale, CA USA. The ALD110900 MOSFET has a nearly zero threshold voltage, making it ideal for designing an oscillator that can operate at a low bias voltage (i.e., as low as 0.121 V). The oscillator can have a compact size of 173 mm^2, as shown in Fig. 2. Fig. 4(b) reports the oscillation frequency against the input RF power, showing a good frequency stability with lower than 5% fluctuations under different input powers. Fig. 4(c) reports the measured temporal waveform of this oscillator in the startup

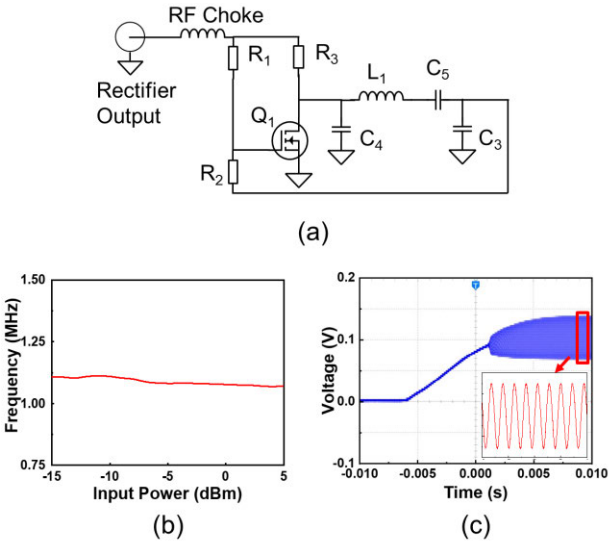

Fig. 4. (a) Schematics of the local oscillator on the intermodulation sensor in Fig. 2(b) and its (b) output frequency at different input RF power levels and (c) temporal waveform at a low dc bias of 0.121 V which corresponded to an RF input power at −13.7 dBm.

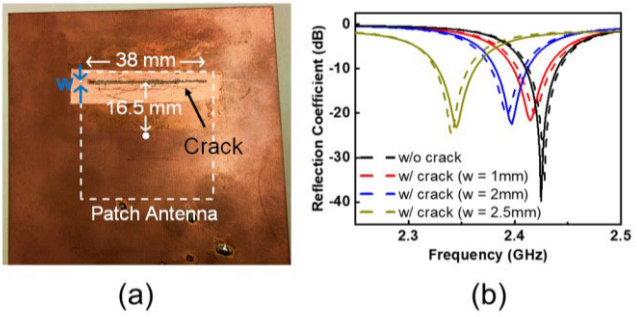

Fig. 5. (a) Photograph of a microstrip patch antenna with a surface crack on its ground plane. (b) Measured (solid lines) and finite-element simulated (dashed lines) reflection spectra of the antenna sensor without (black lines) and with a surface crack; here, the crack is 16.5 mm from the center of the microstrip patch and its dimensions are: length $l = 38$ mm and width $w = 1$ mm (red lines), 2 mm (blue lines), and 2.5 mm (green lines).

phase and the zoomed-in view of the waveform in the normal operation phase at a dc bias of 0.121 V.

C. Crack Sensor Based on Microstrip Patch Antenna

The proposed wireless crack sensor utilizes a microstrip patch antenna as the sensing unit, as shown in Fig. 2; the patch antenna was printed on the Rogers RO4003C substrate with a dielectric constant of 3.55 and a loss tangent of 0.0021, and the cooper patch has a length of 41.8 mm and a width of 38.5 mm. Since a microstrip patch antenna is a high-Q open resonant structure, the slot loading introduced by, for example, a surface crack on the ground plane [see Fig. 5(a)] may lead to a distinct resonance frequency shift. Fig. 5(b) presents the full-wave simulated and measured reflection spectra of a microstrip antenna with and without cracks; here, the surface crack has a length of 38 mm and is 16.5 mm away from the center of the microstrip patch, and its width is varied. To mimic a surface crack on the metallic plate, the bottom

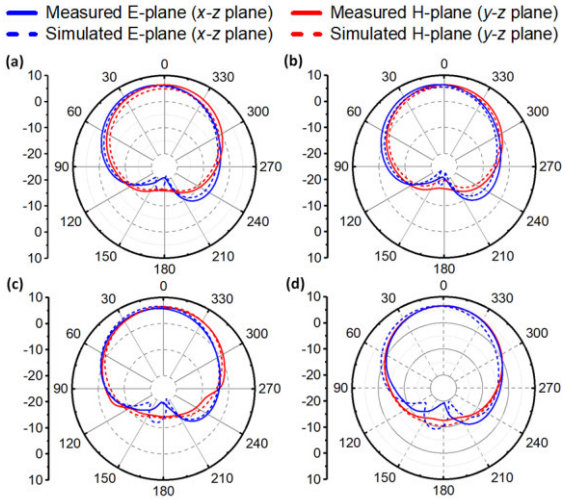

Fig. 6. Experimental and simulation results for the radiation pattern of the microstrip patch antenna (a) without any damage, and with a crack width of (b) 1, (c) 2, and (d) 2.5 mm. In (a)–(d), the antenna was measured at the resonance frequency: 2.42, 2.41, 2.4, and 2.34 GHz, respectively.

layer of the patch antenna was lifted off, as shown in Fig. 5(a). The full-wave simulation was performed using the commercial software ANSYS HFSS, and the numerical results agree well with the experimental results, as can be seen in Fig. 5(b). The measurement results show that the resonance frequency of the microstrip antenna experiences a redshift when the crack width increases. In the absence of cracks, the resonance frequency of the antenna is 2.42 GHz, whereas the resonant frequency of the antenna drops to 2.34 GHz when a crack with a length of 38 mm and a width of 2.5 mm appears.

Fig. 6 presents simulated and measured radiation patterns of the microstrip patch antenna in Fig. 5 without and with a crack on the ground plane. The numerical and experimental results are in good agreement, showing that the presence of cracks of different widths barely affects the radiation pattern and realized gain of the antenna. The measured realized gain is ∼6 dBi and the half-power beamwidth is 91° (102°) on the E-plane (H-plane).

III. Results and Discussion

Fig. 2(a) shows the prototype of an integrated wireless passive crack sensor, which consists of the rectifier/mixer, oscillator, and microstrip patch antenna (i.e., sensing element) reported in Sections I and II. In our wireless measurement setup [Fig. 1(a)], the frequency-hopped RF monotone at f_1 was generated using the vector signal generator (Keysight N5166B CXG), with an output power of 16 dBm from 2.34 to 2.49 GHz. The RF signal was fed to a wideband antenna (RFSPACE UWB3 antenna with a calibrated gain of ∼11 dBi from 2.1 to 3 GHz) through a circulator. The backscattered frequency-modulated signal at $f_1 \pm f_2$ was received by the same antenna and fed to the spectrum analyzer (Keysight N9324C with a noise floor of −90 dBm) through the circulator. The signal generator and the spectrum analyzer were controlled with LabVIEW-based software through VISA

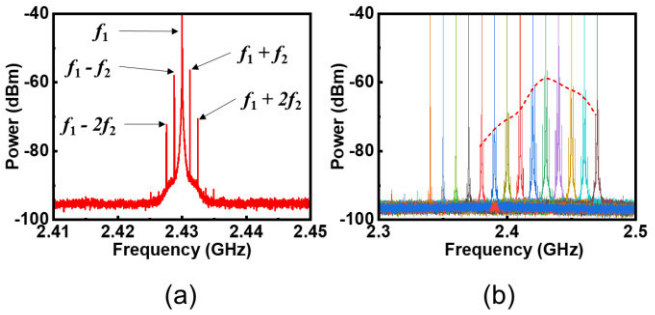

Fig. 7. (a) Received signal strengths at the fundamental (2.45 GHz) and intermodulation frequencies. (b) Received signal strength under frequency hopping from 2.34 to 2.50 GHz. The envelope of the RSSI associated with the antenna's resonance can be exploited to retrieve the cracking condition.

protocol for frequency scanning. The distance between the reader antenna and the passive sensor is 2.45 m.

The proposed passive intermodulation sensor was first measured in an echo/clutter-free anechoic chamber and a noisy indoor environment filled with reflectors and scatters. Fig. 7(a) presents the power spectrum of reflected signals that include the fundamental tone at f_1 (2.43 GHz) and the intermodulation products, $f_1 \pm f_2$ (2.430 GHz $\pm$ 1.08 MHz) and $f_1 \pm 2f_2$ (2.430 GHz $\pm$ 2.16 MHz), for the intermodulation sensor with a crack width of 1 mm. It is evident that intermodulation tones can be generated by the nonlinear sensor placed in the far zone of the interrogator. Fig. 7(b) shows the reflected intermodulation signal at $f_1 - f_2$, for which the f_2 is fixed and f_1 is varied during the FHSS-aided measurement. It can be seen from Fig. 7(b) that the peak frequency of the spectral envelope of reflected intermodulation tones coincides with the antenna's resonance frequency shown in Fig. 5(b). On the other hand, in the indoor measurement, the spectral envelope of reflected fundamental tones shown in Fig. 1(b) exhibits a random and rather chaotic distribution, due to electromagnetic interferences. Such results demonstrate that the proposed intermodulation sensor can be robust against clutters, echoes, jamming, and other interference sources, thanks to the frequency orthogonality between the incident fundamental tone and the reflected intermodulation tone. Moreover, the oscillation frequency (1.08 MHz here) can be regarded as the ID assigned to the sensor. We note that the oscillator can be readily tuned to produce different output frequencies, making it possible to simultaneously interrogate multiple intermodulation sensors with the assistance of the FHSS scheme, which divides the available frequency band into several channels and hops among them in a predetermined order [30].

Fig. 8(a) and (b) reports the measurement setup in an anechoic chamber and the variation of the measured spectral envelope of intermodulation tones $f_1 - f_2$ with respect to the crack size, respectively. Figs. 9–11 are similar to Fig. 8, but for wireless interrogation in a real-world indoor environment with light, moderate, and heavy clutters, respectively. The peak frequency of the spectral envelope of intermodulation tones is determined by the resonance frequency of the microstrip patch antenna, which in turn is varied by the crack size. It can be evidently seen from Figs. 8(b), 9(b), 10(b), and 11(b) that the peak frequency decreases with increasing the crack

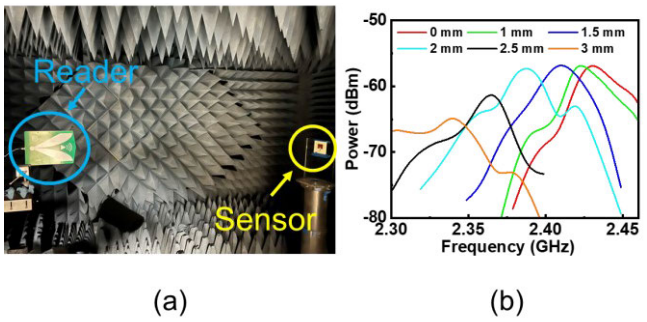

Fig. 8. (a) Wireless readout of the passive intermodulation sensor in the clutter-free anechoic chamber environment. (b) Measurement results for the spectral envelope of intermodulation tones as a function of the crack size.

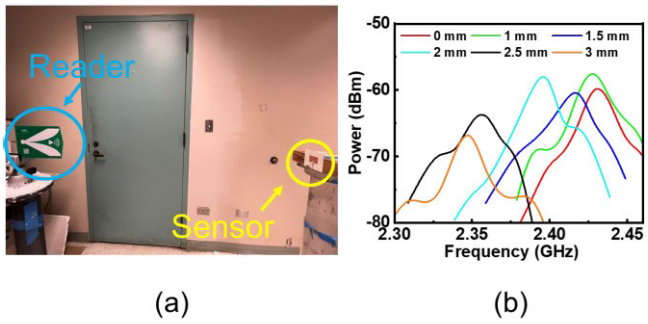

Fig. 9. (a) Wireless readout of the passive intermodulation sensor in the indoor environment. (b) Measurement results for the spectral envelope of intermodulation tones as a function of the crack size.

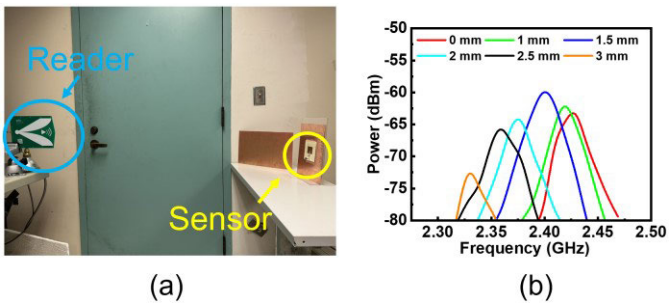

Fig. 10. (a) Wireless readout of the passive intermodulation sensor in a moderately-cluttered environment. (b) Measurement results for the spectral envelope of intermodulation tones as a function of the crack size.

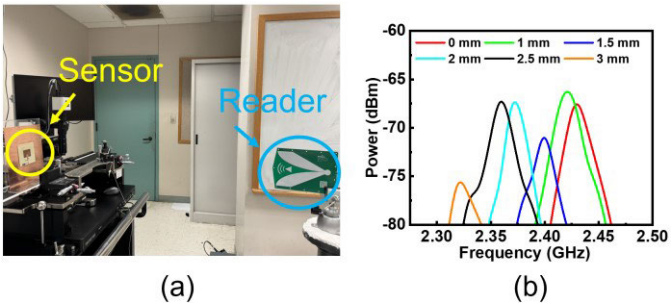

Fig. 11. (a) Wireless readout of the passive intermodulation sensor in a heavily-cluttered environment. (b) Measurement results for the spectral envelope of intermodulation tones as a function of the crack size.

size. Such results are consistent with the measured antenna resonance frequency shift in Fig. 5(b). We should note that although the maximum amplitude of the spectral envelope

TABLE I
SUMMARY OF WIRELESS CRACK DETECTION TECHNIQUES

Technique	Interrogation distance [cm]	Number of antennas required on reader	Number of antennas required on sensor	Clatter-free	Frequency range [GHz]	Chipless
Harmonic RFID [21]	400	2	2	Yes	2-6	Yes
Chip-less RFID [9]	120	2	1	No	4-6	Yes
UHF RFID [31]	37.5	1	1	No	0.865-0.956	No
Coil transducer [32]-[34]	2	1	1	Yes	0-0.006	Yes
FSS [35]	10	1	1	No	2-6	Yes
This work	**200**	**1**	**1**	**Yes**	2.2-2.5	Yes

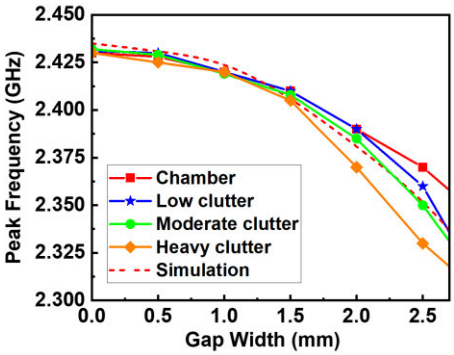

Fig. 12. Peak frequency of the intermodulation RSSI patterns as a function of the crack width; the results were obtained from the full-wave simulation (dashed line) and experiments conducted in the anechoic chamber (rectangle), lightly-cluttered (star), moderately-cluttered (circle), and heavily-cluttered indoor environments (diamond).

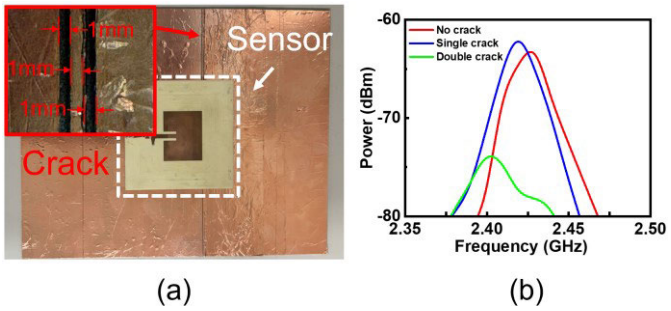

Fig. 13. (a) Photograph and (b) measured intermodulation spectral envelope of the wireless crack sensor in Fig. 2 (without the ground plane). The low-profile sensor is placed conformally on a cracked sample with single or multiple cracks; the inset of (a) shows the zoomed-in view of the crack.

could vary in different wireless propagation scenarios, the frequency at which the magnitude of the spectral envelope has peak remains unchanged, regardless of the density of background clutters and multipath echoes in the noisy environment. Fig. 12 presents the simulated antenna resonance frequency and the measured peak frequencies of intermodulation spectral envelopes under different cracking events. It is evident that the measurement results are in good agreement with the simulation results, indicating that the proposed batteryless, chipless, and wireless sensor, as well as the FHSS-aided, intermodulation-based intermodulation technique can be used to detect cracks accurately and robustly with different severity levels. It is worthwhile mentioning that sensor ID can be achieved by assigning a different oscillation frequency (f_2) to each sensor, which can be readily done by tuning the *LC* resonator of the oscillator. Since the oscillation frequency ranges from tens of kHz to several MHz, it is possible to deploy a massive number of intermodulation sensors in a sensor array. Here, we also removed the ground plane of the intermodulation sensor and placed the sensor on a metal sheet with multiple cracks, as shown in Fig. 13(a). Our measurement results shown in Fig. 13(b) demonstrate that the proposed sensor and system can effectively identify crack(s) for practical wireless SHM applications.

In Table I, we compare various wireless crack detection techniques in terms of the wireless interrogation distance, spectrum efficiency of the sensing system (i.e., the throughput supported by per bandwidth usage), requirement of RFID/Near Field Communication (NFC) chipsets, and size/design complexity of reader and sensor (i.e., relative to the number of antennas). We note that the proposed intermodulation sensor possesses several advantages when compared with current wireless crack sensors. First, it can have an elongated interrogation range than those based on inductive coupling (e.g., coil antennas) or chip-loaded RFIDs that necessitate sufficiently large energy to power up the digital memory and processor. In addition, compared to other clutter-resistive passive wireless sensors such as harmonic RFIDs, it eliminates the need for multispectrum operation and, therefore, requires only a single reader/sensor antenna and gets rid of at least one stage of filter and matching network. This will not only improve the spectrum efficiency of the sensing system, but also significantly reduce the cost, size, and design complexity of the reader. More interestingly, it is possible to identify sensors in an array by identifying the oscillation frequency assigned to each sensor tag.

IV. CONCLUSION

We have proposed and verified experimentally a new concept of passive intermodulation sensor that can be effective in noise suppression and enable nonvolatile memory-free ID. As proof of concept, we have implemented and characterized an intermodulation sensor for real-time monitoring of mechanical cracks in clutter-free and cluttered environments.

Compared with other clutter-resistive passive sensors, such as harmonic transponder sensors, the proposed intermodulation sensor can have a more compact size by removing the antenna operating at the harmonic frequency and at least one stage of filter and matching network. Moreover, the intermodulation-based interrogation scheme can significantly ease the design complexity and cost of the interrogator by eliminating the need for multispectrum operation. Additionally, the sensor ID can be encoded in the kHz/MHz oscillation frequency, thereby enabling the deployment of sensor arrays for practical SHM. We envision that such a compact, low-noise, battery-less (maintenance-free), wireless, and chipless intermodulation sensor may be beneficial for practical SHM and NDE, facilitating the preventive maintenance scheduling of civil infrastructures, aircrafts, vehicles, manufacturing facilities, and smart cities connected via 5G.

REFERENCES

[1] Y. Yao, S.-T.-E. Tung, and B. Glisic, "Crack detection and characterization techniques—An overview," *Struct. Control Health Monitor.*, vol. 21, no. 12, pp. 1387–1413, Mar. 2014.

[2] B. Beral and H. Speckmann, "Structural health monitoring (SHM) for aircraft structures: A challenge for system developers and aircraft manufacturers," in *Proc. 4th Int. Workshop Struct. Health Monitor.*, F.-K. Chang, Ed. Stanford, CA, USA: Stanford Univ., 2003, p. 12.

[3] Y. Q. Ni, X. G. Hua, and J. M. Ko, "Reliability-based assessment of bridges using long-term monitoring data," *Key Eng. Mater.*, vols. 321–323, pp. 217–222, Oct. 2006.

[4] K. Chintalapudi et al., "Monitoring civil structures with a wireless sensor network," *IEEE Internet Comput.*, vol. 10, no. 2, pp. 26–34, Mar. 2006.

[5] J. Zhang, G. Y. Tian, and A. B. Zhao, "Passive RFID sensor systems for crack detection & characterization," *NDT E Int.*, vol. 86, pp. 89–99, Mar. 2017.

[6] S. Sony, S. Laventure, and A. Sadhu, "A literature review of next-generation smart sensing technology in structural health monitoring," *Struct. Control Health Monitor.*, vol. 26, no. 3, p. e2321, Jan. 2019.

[7] B. F. Spencer, M. Ruiz-Sandoval, and N. Kurata, "Smart sensing technology for structural health monitoring," in *Proc. 13th World Conf. Earthquake Eng.*, Vancouver, BC, Canada, Aug. 2004, pp. 1–6.

[8] M. Abdulkarem, K. Samsudin, F. Z. Rokhani, and M. F. A. Rasid, "Wireless sensor network for structural health monitoring: A contemporary review of technologies, challenges, and future direction," *Struct. Health Monitor.*, vol. 19, no. 3, pp. 693–735, Jul. 2019.

[9] A. M. J. Marindra and G. Y. Tian, "Chipless RFID sensor tag for metal crack detection and characterization," *IEEE Trans. Microw. Theory Techn.*, vol. 66, no. 5, pp. 2452–2462, May 2018.

[10] A. M. J. Marindra and G. Y. Tian, "Multiresonance chipless RFID sensor tag for metal defect characterization using principal component analysis," *IEEE Sensors J.*, vol. 19, no. 18, pp. 8037–8046, Sep. 2019.

[11] P. Kalansuriya, R. Bhattacharyya, and S. Sarma, "RFID tag antenna-based sensing for pervasive surface crack detection," *IEEE Sensors J.*, vol. 13, no. 5, pp. 1564–1570, May 2013.

[12] I. Mohammad, V. Gowda, H. Zhai, and H. Huang, "Detecting crack orientation using patch antenna sensors," *Meas. Sci. Technol.*, vol. 23, no. 1, Nov. 2011, Art. no. 015102.

[13] C. Gu, J. A. Rice, and C. Li, "A wireless smart sensor network based on multi-function interferometric radar sensors for structural health monitoring," in *Proc. IEEE Topical Conf. Wireless Sensors Sensor Netw.*, Santa Clara, CA, USA, Jan. 2012, pp. 33–36.

[14] P. Kamalinejad, C. Mahapatra, Z. Sheng, S. Mirabbasi, V. C. M. Leung, and Y. L. Guan, "Wireless energy harvesting for the Internet of Things," *IEEE Commun. Mag.*, vol. 53, no. 6, pp. 102–108, Jun. 2015.

[15] H.-C. Liu, M.-C. Hua, C.-G. Peng, and J.-P. Ciou, "A novel battery-assisted class-1 generation-2 RF identification tag design," *IEEE Trans. Microw. Theory Techn.*, vol. 57, no. 5, pp. 1388–1397, May 2009.

[16] H. A. Sodano, "Development of an automated eddy current structural health monitoring technique with an extended sensing region for corrosion detection," *Struct. Health Monitor.*, vol. 6, no. 2, pp. 111–119, Jun. 2007.

[17] Y. He, G. Tian, H. Zhang, M. Alamin, A. Simm, and P. Jackson, "Steel corrosion characterization using pulsed eddy current systems," *IEEE Sensors J.*, vol. 12, no. 6, pp. 2113–2120, Jun. 2012.

[18] J.-B. Ihn and F.-K. Chang, "Pitch-catch active sensing methods in structural health monitoring for aircraft structures," *Struct. Health Monitor.*, vol. 7, no. 1, pp. 5–19, Mar. 2008.

[19] Y. Yang, C.-T. Ng, A. Kotousov, H. Sohn, and H. J. Lim, "Second harmonic generation at fatigue cracks by low-frequency Lamb waves: Experimental and numerical studies," *Mech. Syst. Signal Process.*, vol. 99, pp. 760–773, Jan. 2018.

[20] Y. Shen and V. Giurgiutiu, "Predictive modeling of nonlinear wave propagation for structural health monitoring with piezoelectric wafer active sensors," *J. Intell. Mater. Syst. Struct.*, vol. 25, no. 4, pp. 506–520, Mar. 2014.

[21] L. Zhu, H. Huang, M. M.-C. Cheng, and P.-Y. Chen, "Compact, flexible harmonic transponder sensor with multiplexed sensing capabilities for rapid, contactless microfluidic diagnosis," *IEEE Trans. Microw. Theory Techn.*, vol. 68, no. 11, pp. 4846–4854, Nov. 2020.

[22] L. Zhu, M. Farhat, Y.-C. Chen, K. N. Salama, and P.-Y. Chen, "A compact, passive frequency-hopping harmonic sensor based on a microfluidic reconfigurable dual-band antenna," *IEEE Sensors J.*, vol. 20, no. 21, pp. 12495–12503, Nov. 2020.

[23] M. Yang, Z. Ye, M. Farhat, and P.-Y. Chen, "Ultrarobust wireless interrogation for sensors and transducers: A non-hermitian telemetry technique," *IEEE Trans. Instrum. Meas.*, vol. 70, pp. 1–9, 2021.

[24] X. Hui and E. C. Kan, "Monitoring vital signs over multiplexed radio by near-field coherent sensing," *Nature Electron.*, vol. 1, no. 1, pp. 74–78, Nov. 2017.

[25] X. Gu, W. Lin, S. Hemour, and K. Wu, "Readout distance enhancement of battery-free harmonic transponder," *IEEE Trans. Microw. Theory Techn.*, vol. 69, no. 7, pp. 3413–3424, Jul. 2021.

[26] D. M. Pozar, *Microwave Engineering*, 4th ed. New York, NY, USA: Wiley, 2011, pp. 306–312.

[27] R. G. Carter, "Accuracy of microwave cavity perturbation measurements," *IEEE Trans. Microw. Theory Techn.*, vol. 49, no. 5, pp. 918–923, May 2001.

[28] H.-M. Lee and M. Ghovanloo, "An adaptive reconfigurable active voltage doubler/rectifier for extended-range inductive power transmission," *IEEE Trans. Circuits Syst. II, Exp. Briefs*, vol. 59, no. 8, pp. 481–485, Aug. 2012.

[29] A. G. Radwan, A. M. Soliman, and A. S. Elwakil, "Design equations for fractional-order sinusoidal oscillators: Four practical design examples," *Int. J. Circuit Theory Appl.*, vol. 36, pp. 473–492, Jun. 2008.

[30] C. A. Balanis, *Antenna Theory: Analysis and Design*. Hoboken, NJ, USA: Wiley, 2016.

[31] O. Salim, S. Dey, H. Masoumi, and N. C. Karmakar, "Crack monitoring system for soft rock mining conveyor belt using UHF RFID sensors," *IEEE Trans. Instrum. Meas.*, vol. 70, pp. 1–12, 2021.

[32] W. Wang et al., "Novel coil transducer induced thermoacoustic detection of rail internal defects towards intelligent processing," *IEEE Trans. Ind. Electron.*, vol. 71, no. 2, pp. 2100–2111, Feb. 2024.

[33] W. Wang et al., "Analysis and design of coil-based electromagnetic-induced thermoacoustic for rail internal-flaw inspection," *IEEE Trans. Intell. Transp. Syst.*, vol. 20, no. 7, pp. 2691–2702, Jul. 2019.

[34] W. Wang et al., "MRC-based double figure-of-eight coil sensor system with triple-mode operation capability for biomedical applications," *IEEE Sensors J.*, vol. 21, no. 13, pp. 14491–14502, Jul. 2021.

[35] S.-D. Jang, B.-W. Kang, and J. Kim, "Frequency selective surface based passive wireless sensor for structural health monitoring," *Smart Mater. Struct.*, vol. 22, no. 2, Dec. 2012, Art. no. 025002.

Xuecong Nie received the bachelor's degree from the Huazhong University of Science and Technology, Wuhan, China, in 2016, and the master's degree from the University of Michigan at Dearborn, Dearborn, MI, USA, in 2019. He is pursuing the Ph.D. degree with the Department of Electrical and Computer Engineering, University of Illinois Chicago (UIC), Chicago, IL, USA.

Nanshu Wu is pursuing the Ph.D. degree with the Department of Electrical and Computer Engineering, University of Illinois Chicago (UIC), Chicago, IL, USA.

His research interests include applied electromagnetics and related problems.

Chung-Tse Michael Wu (Senior Member, IEEE) received the B.S. degree in electrical engineering from National Taiwan University (NTU), Taipei, Taiwan, in 2006, and the M.S. and Ph.D. degrees in electrical engineering from the University of California at Los Angeles (UCLA), Los Angeles, CA, USA, in 2009 and 2014, respectively.

From September 2008 to June 2014, he was a Graduate Student Researcher with the Microwave Electronics Laboratory, UCLA. In 2009, he joined the Bell Labs, Murray Hill, NJ, USA, as a Summer Intern. In 2012, he joined the Japan Aerospace Exploration Agency (JAXA), Sagamihara, Japan, as a Special-Joint Researcher. From 2014 to 2017, he was an Assistant Professor with the Department of Electrical and Computer Engineering, Wayne State University (WSU), Detroit, MI, USA. He is currently an Assistant Professor with Rutgers University, New Brunswick, NJ. His research interests include applied electromagnetics, antennas, passive/active microwave and millimeter-wave components, RF systems, and metamaterials.

Dr. Wu was a recipient of the National Science Foundation (NSF) Faculty Early Career Development (CAREER) Award, the WSU College of Engineering Faculty Research Excellence Award in 2016, Defense Advanced Research Projects Agency (DARPA) Young Faculty Award (YFA) in 2019, and DARPA Director's Fellowship Award in 2021. He is currently serving as the Secretary for IEEE Princeton Central Jersey Section (PCJS), as well as the Vice-Chair for the IEEE PCJS Joint AP/ED/MTT Chapter. He is also the Vice-Chair and a Technical Program Committee Member of IEEE MTT-28: Biological Effects and Medical Applications of RF and Microwaves.

Pai-Yen Chen (Senior Member, IEEE) received the B.S. and M.S. degrees from National Chiao Tung University, Hsinchu, Taiwan, in 2004 and 2006, respectively, and the Ph.D. degree from The University of Texas at Austin, Austin, TX, USA, in 2013.

He was a Research Staff with the Taiwan Semiconductor Research Institute, Tainan, Taiwan, from 2006 to 2009. He was a Research Scientist with the Intellectual Ventures' Metamaterial Commercialization Center, Bellevue, WA, USA, from 2013 to 2014. He is an Associate Professor with the Department of Electrical and Computer Engineering, University of Illinois Chicago (UIC), Chicago, IL, USA. He has been involved in multidisciplinary research on applied electromagnetics, RF and microwave antennas and circuits, wireless sensors and systems, nanoelectronics, nanophotonics, plasmonics, metamaterials, and metasurfaces.

Dr. Chen has received quite a few prestigious awards, including IEEE Sensors Distinguished Lecturer for the period 2024–2026, National Science Foundation (NSF) CAREER Award, IEEE Sensors Council Young Professional Award, IEEE Raj Mittra Travel Grant (RMTG) Award, IEEE Chicago Distinguished Senior Research and Development Award, SPIE Rising Researcher Award, ACES Early Career Award, PIERS Young Scientist Award, Young Scientist Awards from URSI General Assembly and URSI Commission B: Electromagnetics, IOP Emerging Leader in Measurement Science and Technology, Air Force Research Laboratory Faculty Fellowship, UIC College of Engineering Faculty Research Award, College of Engineering Faculty Research Excellence Award, Donald Harrington Fellowship, Taiwan Ministry of Education Study Abroad Award, United Microelectronics Corporation Scholarship, the best student paper awards/finalists from the IEEE Antennas and Propagation Symposium in 2011, 2013, 2016, and 2021, IEEE International Microwave Symposium in 2015, IEEE Sensors Conference in 2016, and IEEE Wireless Power Transfer Conference in 2021, USNC-URSI Ernest K. Smith Student Paper Award in 2012, and Second Prize of the Student Design Contest from the IEEE Antennas and Propagation Symposium in 2022. He currently serves as an Associate Editor for IEEE SENSORS JOURNAL, IEEE TRANSACTIONS ON ANTENNAS AND PROPAGATION, and IEEE ANTENNAS AND WIRELESS PROPAGATION LETTERS, and a Guest Editor for IEEE JOURNAL OF SELECTED AREAS IN SENSORS. He was a former Associate Editor of *Applied Electromagnetics*, IEEE JOURNAL OF RADIO FREQUENCY IDENTIFICATION, and IEEE JOURNAL OF ELECTROMAGNETICS, RF AND MICROWAVES IN MEDICINE AND BIOLOGY (IEEE-JERM), and a former Guest Editor of IEEE TRANSACTIONS ON ANTENNAS AND PROPAGATION. He currently serves as the Chair for IEEE Chicago AP-S/MTT-S Joint Chapter. He was the Chair/Founder of IEEE Chicago Sensors Chapter from 2019 to 2021 and the ACES Board of Directors from 2021 to 2023.